RESEARCH ARTICLE

Key Points:
- Intensity of surface reflections is a proxy for low-altitude electron densities
- Intensity of surface reflections lower at higher SZAs and during solar maximum
- Intensity of surface reflections lower at areas of closed magnetic field lines

Correspondence to:
F. Němec,
frantisek.nemec@gmail.com

Intensity of nightside MARSIS AIS surface reflections and implications for low-altitude ionospheric densities

F. Němec[1], D. D. Morgan[2], C. Diéval[2], and D. A. Gurnett[2]

[1]Faculty of Mathematics and Physics, Charles University in Prague, Prague, Czech Republic, [2]Department of Physics and Astronomy, University of Iowa, Iowa City, Iowa, USA

Abstract Spacecraft radar sounding signals at frequencies higher than the ionospheric peak plasma frequency are not reflected by the ionosphere. Instead, they make it to the ground where they are reflected by the planetary surface. We analyze the intensity of the surface reflections measured by the Mars Advanced Radar for Subsurface and Ionosphere Sounding (MARSIS) ionospheric radar sounder on board the Mars Express spacecraft. Apart from the surface reflectivity and the spacecraft altitude, the detected intensity of surface reflections is controlled primarily by the signal attenuation during the ionospheric propagation. We focus on the nightside region, where the ionospheric densities in the main layer are too low to cause a significant attenuation and allow sampling of the surface reflections at frequencies down to 3 MHz. The attenuation occurs mainly at altitudes below 100 km, where the electron-neutral collision frequency is a maximum. The intensity of surface reflections can thus serve as a proxy for electron densities at low altitudes not accessible by the direct ionospheric radar sounding. We analyze the intensity of surface reflections as a function of relevant controlling parameters. The intensity of surface reflections is lower at higher solar zenith angles on the nightside and during the periods of larger solar activity. Moreover, it exhibits a seasonal variation that is related to the dust storm occurrence. The intensity of surface reflections is lower in areas of closed magnetic field lines, suggesting that nightside electron densities behave rather differently at low altitudes than at higher altitudes. This is confirmed by comparison with simultaneous observations of the main ionospheric layer.

1. Introduction

Experimental information about electron densities in the nightside ionosphere of Mars remains rather limited. The electron densities are often too low to be properly detected, e.g., only less than 10% of nightside ionograms obtained by the MARSIS radar sounder on board the Mars Express spacecraft contain a signature of the ionospheric reflection [*Němec et al.*, 2010]. Moreover, due to geometric constraints imposed by the orbits of Earth and Mars, radio occultation measurements are restricted to solar zenith angles (SZAs) lower than about 132°. Any experimental information related to the Martian nightside ionosphere is therefore welcome. In the present paper we use the ionospheric attenuation of the Mars Advanced Radar for Subsurface and Ionosphere Sounding (MARSIS) signal as an integral characteristic related to ionospheric electron densities, being most sensitive to electron densities at low altitudes.

The basic idea is that only radar sounding signals at frequencies lower than the maximum plasma frequency throughout the ionosphere are reflected by the ionosphere. If the sounding frequency is larger than the ionospheric peak plasma frequency, the sounding signal is not reflected by the ionosphere. Instead, it makes it to the ground, where it is reflected by the planetary surface. The reflected signal is then detected by the radar sounder, and it results in a surface reflection signature observable in MARSIS ionograms [*Gurnett et al.*, 2005]. However, the signal encounters a two-way (to the ground and back) attenuation during the ionospheric propagation. The evaluation of the observed ground trace intensities thus provides a measure of the wave attenuation in the ionosphere, which is directly related to electron density and electron-neutral collision frequency profiles. It will be these reflections of the sounding signal from the planetary surface and their intensity that we will analyze in the present paper.

Morgan et al. [2006] used the data measured by the MARSIS radar sounder in the ionospheric sounding mode at SZAs larger than 50° to check whether the ionospheric attenuation is large enough to prevent surface

reflection from being detected or not. They showed that while under normal conditions the sounding signal reflected from the planetary surface is easily detectable, it principally disappears during time intervals of increased influx of high-energy solar protons. These high-energy protons increase the electron density in the Martian ionosphere and thus the wave attenuation. The region particularly important for this additional attenuation is located at altitudes below about 100 km, where the neutral densities are high (and thus electron-neutral collision frequencies are high [e.g., *Nielsen et al.*, 2007]), and even a comparatively small additional ionization therefore results in a significantly increased attenuation [e.g., *Nielsen et al.*, 2007; *Withers*, 2011]. A similar result was obtained by *Espley et al.* [2007] using the subsurface sounding data. The analysis of the sounding signal absorption was further used by *Morgan et al.* [2010] to analyze the encounter of a corotating interaction region with Mars and by *Morgan et al.* [2014] to analyze effects of a strong interplanetary coronal mass ejection on the Martian ionosphere. As the ionospheric attenuation is lower for higher sounding frequencies [*Witasse et al.*, 2001], it is possible to analyze not only the visibility of the ground trace as a whole but also the lowest frequency of observed surface reflections. The obtained results were compared with the expected dependence calculated assuming the Chapman layer on the dayside, and the observations were found to be consistent with predictions [*Nielsen et al.*, 2007]. *Němec et al.* [2014] analyzed nightside ionospheric electron densities and surface reflection visibility during 15 solar energetic particle (SEP) events identified in the background counts data recorded by the ion sensor of the ASPERA-3 instrument on board Mars Express. They showed that during the SEP events the reflections of the sounding signal from the ground almost entirely disappear, indicating a substantial ionization at altitudes below about 80 km [*Sheel et al.*, 2012].

The first attempt to quantify the expected attenuation of a radar signal by the Martian ionosphere was performed by *Witasse et al.* [2001]. They concluded that especially for lower sounding frequencies and during the daytime, the ionospheric attenuation may be rather significant. Further analysis of the radar signal distortion was performed by *Safaeinili et al.* [2003], who analyzed not only the signal attenuation but also its dispersion and Faraday rotation. Most recently, a thorough theoretical investigation of the radar signal attenuation in the Martian ionosphere was conducted by *Withers* [2011]. He developed theoretical expressions for the attenuation caused by an ionospheric plasma layer at different approximations, and he applied these relationships to the layers existing at Mars. The important point stemming from his analysis is that the nightside electron densities are generally too low ($< 10^4$ cm^{-3} [*Němec et al.*, 2010]) to cause a significant attenuation at the expected peak altitudes of about 160 km [*Lillis et al.*, 2009]. On the other hand, even much lower electron densities can cause a significant attenuation if optimally located at lower altitudes [see *Withers*, 2011, Figure 3].

We present results of a systematic analysis of intensity of nightside surface reflections measured by the MARSIS ionospheric radar sounder on board the Mars Express spacecraft. Since the attenuation of the sounding signal takes place mostly at lower altitudes, the detected intensity of surface reflections serves as a proxy for the low-altitude ionospheric densities. The used data set and the applied data processing are described in section 2. The obtained results are presented in section 3 and discussed in section 4. Finally, the main results are briefly summarized in section 5.

2. Data Set and Processing

We have used data acquired by the Mars Express spacecraft, which is in an elliptical orbit around Mars with a periapsis altitude of about 275 km and an apoapsis altitude of about 11,000 km [*Chicarro et al.*, 2004]. The data were measured by the MARSIS radar sounder, which is an instrument designed for topside ionospheric sounding. In the used ionospheric sounding mode, there are 160 sounding frequencies quasi-logarithmically spaced from 0.1 to 5.5 MHz. The intensities of detected echoes are recorded in 80 equally spaced time delay bins over an interval of 7.31 ms. More detailed descriptions of the MARSIS instrument and the related data processing were given by *Picardi et al.* [2004], *Gurnett et al.* [2005], *Jordan et al.* [2009], and *Morgan et al.* [2013].

The basic idea of the ionospheric sounding is that the sounding signal of a frequency f cannot propagate in the plasma environment with the plasma frequency $f_p > f$. A wave entering such a region is therefore reflected. The reflected signal is then detected by the sounding spacecraft, and the time delay between the signal transmission and the detection of the reflected ionospheric echo is evaluated. Varying the sounding frequency and assuming that the ionospheric electron density increases monotonically with decreasing altitude, the topside ionospheric sounding allows us to obtain electron density profiles from the spacecraft altitude down to the altitude of the peak electron density [*Morgan et al.*, 2013]. However, if the sounding frequency is higher than the peak plasma frequency in the ionosphere ($f > f_p^{max}$), the sounding signal is not
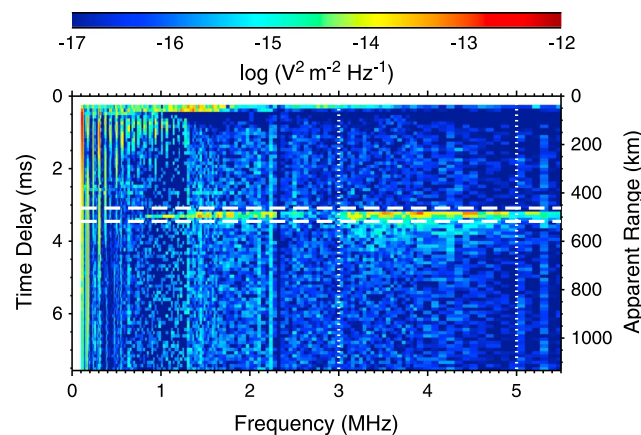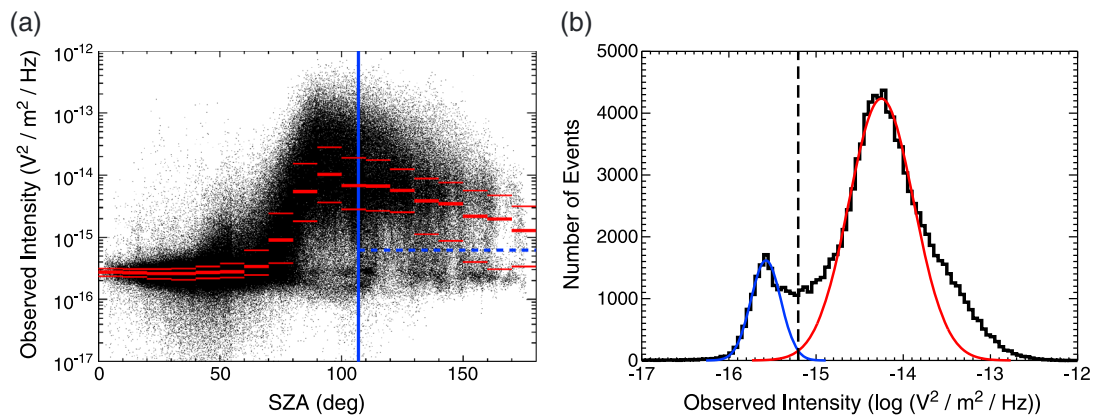
Figure 1. Example of an ionogram with a signature of the signal reflected from the ground. Received intensity is color coded as a function of the sounding frequency (abscissa) and time delay (left-hand ordinate) or apparent range (right-hand ordinate). The ground trace is the area of enhanced intensity at time delays marked by two horizontal white dashed lines, spanning all but lowest sampled frequencies. The frequency interval of the sounding signal (3–5 MHz) analyzed in the present study is marked by vertical white dotted lines.

reflected by the ionosphere. Instead, it propagates all the way down to the planetary surface, where it gets reflected [*Gurnett et al.*, 2005]. The signal reflected from the planetary surface is then detected by the sounding spacecraft. However, during the propagation path, it suffers a two-way attenuation. When we have accounted for geographic variations of the surface reflectivity (see further below), the intensity of surface reflections thus provides information about the state of the ionosphere even at altitudes below the peak altitude, i.e., in the region normally inaccessible by the ionospheric sounding. However, as compared to total electron content values [*Safaeinili et al.*, 2007; *Mouginot et al.*, 2008], which are equally sensitive to electron densities at all altitudes, the sounding signal attenuation is primarily sensitive to electron densities at lower altitudes, because the electron-neutral collision frequency is highest there [*Witasse et al.*, 2001].

Figure 1 shows an example of a MARSIS ionogram which contains a signature of the signal reflected from the ground (ground trace). The measured intensity is color coded as a function of the sounding frequency (abscissa) and time delay (left-hand ordinate) or apparent range (right-hand ordinate). The ground trace is the area of enhanced intensity at time delays marked by two horizontal white dashed lines, which spans all but the lowest sampled frequencies. The time delays corresponding to the horizontal white dashed lines were calculated directly from the known spacecraft altitude. Specifically, the upper white dashed line (lower estimate of the ground trace time delay) was calculated as twice the spacecraft altitude over the speed of light. The time delay interval between white dashed lines corresponds to four time delay bins, which is an empirically found time delay corresponding to the ground trace "thickness" due to the signal dispersion and scattering. It should be noted that if the sounding frequency is close to but still above the peak ionospheric plasma frequency, the dispersion becomes so large that the ground trace is no longer flat but rather exhibits a cusplike structure in the apparent altitude. Nevertheless, the ground traces considered in this work are typically flat, because the analysis is limited to higher sounding frequencies and the nightside, where the peak plasma frequencies are generally rather low. There are two principal reasons that the ground trace is not observed at the lowest sampled frequencies: (i) the lowest observable frequency of the ground trace must be higher than the ionospheric peak plasma frequency throughout the ionosphere and (ii) the power radiated by MARSIS is very low at low frequencies due to the f^4 frequency dependence of the radiation from a dipole at low frequencies. As the power radiated by MARSIS somewhat decreases also at high sounding frequencies, the ground trace intensity is typically largest at frequencies from about 3 to 5 MHz. We will focus in our further analysis exclusively on this frequency range, marked by the vertical white dotted lines in Figure 1. We note that the plasma frequency of 3 MHz corresponds to electron densities of more than $10^5 \, \text{cm}^{-3}$, which is larger than the maximum peak electron density in the Martian nightside ionosphere observed by MARSIS during several years of operation [*Němec et al.*, 2010]. The analyzed frequency range of 3–5 MHz thus ensures that we analyze exclusively the signals reflected from the planetary surface.

Having determined the time delay interval and the frequency range of the ground trace, we define its overall intensity as a sum over the four time delay bins and an average over frequencies in the 3–5 MHz range. The resulting ground trace intensities are shown in Figure 2a as a function of SZA. Median values of ground trace intensities calculated over given SZA intervals are shown by thick solid red lines, and 0.25 and 0.75 quartiles calculated over the same SZA intervals are shown by thinner solid red lines. It can be seen that the intensity is very low on the dayside, and it gradually increases toward the terminator. This is approximately the expected

Figure 2. (a) Observed ground trace intensity as a function of SZA. Median values calculated over given SZA intervals are shown by thick solid red lines, and 0.25 and 0.75 quartiles calculated over the same SZA intervals are shown by thinner solid red lines. Only nightside data at SZA > 107° (to the right from the vertical blue solid line) are used in the further analysis. Horizontal blue dashed line determined using the analysis in Figure 2b separates the intensities corresponding to the noise-only situation (below the line). (b) Histogram of ground trace intensities at SZA > 107°. Its two peaks were fitted by Gaussian functions, and the threshold intensity separating the peaks is marked by the vertical black dashed line.

behavior. Near the subsolar point, the ionospheric densities in the main layer are so large that ground traces are not observable in MARSIS ionograms. Low ground trace intensities obtained at low SZAs are thus not realistic, as they correspond principally only to the noise level. The increase of the ground trace intensity when approaching the terminator is due to the decrease of the electron density in the main layer [*Nielsen et al.*, 2007; *Mouginot et al.*, 2010]. Ground trace intensities on the nightside decrease with increasing SZA. This is partly due to the sampling bias, as the data points at high SZAs were typically obtained at times when the spacecraft altitude was rather high, resulting in lower ground trace intensities (see below). Nevertheless, even when accounting for the varying spacecraft altitude, this effect remains, and it appears to be real. A more detailed analysis of this interesting unexpected phenomenon is performed in section 3.

The peak electron densities on the nightside are generally lower than 10^4 cm^{-3} [*Němec et al.*, 2010], and the peak altitudes are about 160 km [*Lillis et al.*, 2009], i.e., little attenuation of the signal occurs in the main layer of the nightside ionosphere [*Withers*, 2011]. Nevertheless, a significant attenuation may occur at low altitudes ($\approx$ 60 km), provided that the electron densities in the region are reasonably high ($>10^2$ cm^{-3}). The evaluation of the nightside signal attenuation is thus related to the electron densities at low altitudes, which are otherwise inaccessible by the topside ionospheric sounding. We will therefore focus exclusively on the analysis of the intensities of ground traces observed on the nightside (SZA > 107°), i.e., in the region to the right of the vertical solid blue line in Figure 2a. Moreover, the data obtained at the times of 15 SEP events identified by *Němec et al.* [2014] were excluded from the analysis, as SEP events are known to cause extremely large ionization at low altitudes, resulting in ground traces not being observable [*Morgan et al.*, 2006; *Němec et al.*, 2014].

A histogram of the observed nightside ground trace intensities is shown in Figure 2b. It has two distinct peaks. The peak at lower intensities corresponds to the situation when the attenuation of the sounding signal during the ionospheric propagation is so large that the ground trace is not identifiable in MARSIS ionograms, i.e., the calculated ground trace intensity corresponds to the noise-only situation. The peak at higher intensities corresponds to MARSIS ionograms with identifiable ground trace reflections. It is of interest to find a threshold intensity dividing the two peaks, because ground trace intensities lower than this threshold should be effectively considered as equal to zero. Both peaks are approximated by a Gaussian function, and the appropriate intensity threshold value is determined as the intensity where the Gaussian fits intersect, $I_0 = 10^{-15.2}$ V^2 m^{-2} Hz^{-1}. This intensity threshold is overplotted by the vertical black dashed line in Figure 2b and the horizontal blue dashed line in Figure 2a. All ground trace intensities $I < I_0$ are set to zero, as they do not correspond to the real signal reflected from the planetary surface, but only to background noise.

The observed ground trace intensities are shown in Figure 3a as a function of the spacecraft altitude. Median values calculated over given altitudinal ranges are shown by thick solid red lines, and 0.25 and 0.75 quartiles calculated over the same altitudinal intervals are shown by thinner solid red lines. It can be seen that the observed ground trace intensities decrease with the spacecraft altitude. This is an expected effect due to the varying spatial separation and the nonzero beam divergence of the sounding signal, and we can readily
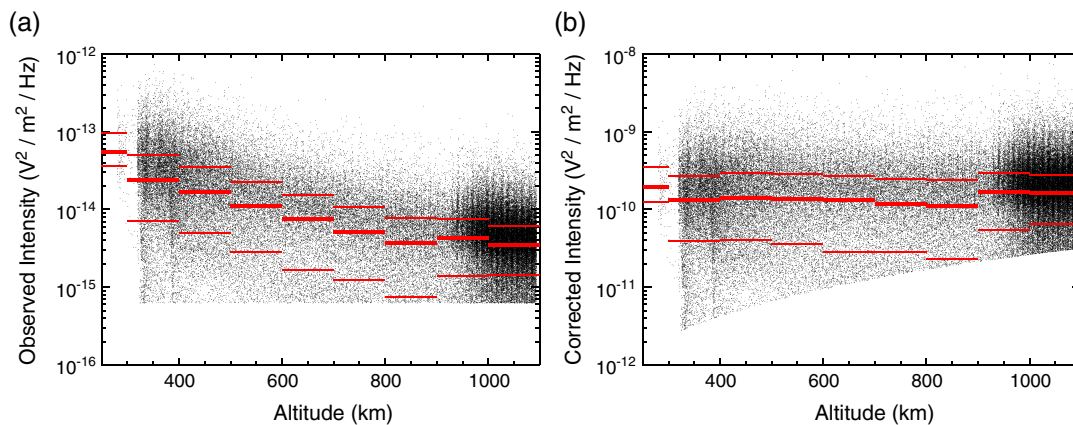
Figure 3. (a) Observed ground trace intensity as a function of the spacecraft altitude is shown by black points. Median values calculated over given altitudinal ranges are shown by thick solid red lines, and 0.25 and 0.75 quartiles calculated over the same altitudinal intervals are shown by thinner solid red lines. (b) Corrected intensity, i.e. the ground trace intensity corrected for the altitudinal effect, as a function of the spacecraft altitude. The used format is the same as in panel (a).

correct for it using equation (6) of *Nielsen et al.* [2007]. The resulting corrected ground trace intensity, i.e., the ground trace intensity divided by the attenuation factor due to the spatial separation, is shown in Figure 3b as a function of the spacecraft altitude. The format of the figure is the same as the format of Figure 3a. Unlike the observed ground trace intensities, corrected ground trace intensities are basically independent of the spacecraft altitude. It should be noted that the reason for the sharp lower cutoffs in Figures 3a and 3b stems from the setting of the intensity values lower than I_0 to zero. These intensity cutoffs thus correspond to the minimum ground trace intensities that are still observable at a given spacecraft altitude.

In order to enable a comparison of the ionospheric attenuation derived from the ground trace intensities observed at different locations, a normalization taking into account geographic variations of the surface reflectivity needs to be taken into account. The surface reflectivity varies both because of varying surface roughness and varying surface dielectric constant [*Mouginot et al.*, 2010; *Grima et al.*, 2012]. However, for our purpose, it is meaningless to try to distinguish between these two factors, and it is sufficient to take into account only the overall reflectivity of the surface at a given point. The best way to account for the varying overall surface reflectivity is the analysis of the ground trace intensities themselves. We assume that the over-all surface reflectivity remains about constant on spatial scales of 5°. This assumption is necessary to ensure a sufficient number of data points (hundreds) measured in a given location. For each corrected ground trace intensity, we calculate the median value of corrected ground trace intensities obtained within 5° of a given
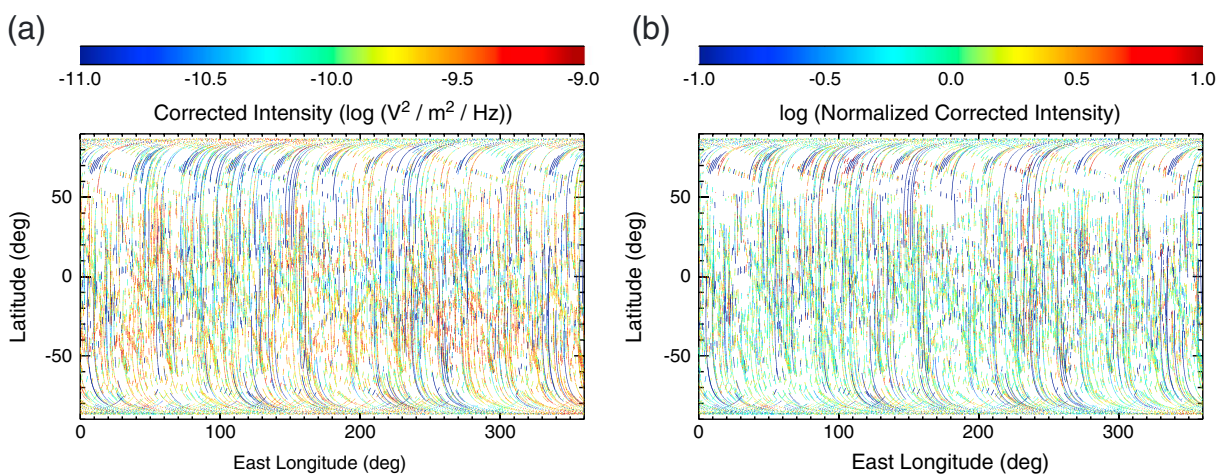
Figure 4. (a) Geographic locations where the analyzed ionograms were measured. Color coded using the scale at the top is the corrected intensity of ground traces observed at individual locations. (b) The same as in Figure 4a but for the corrected intensity of ground traces normalized by the median corrected intensity of nearby data points.
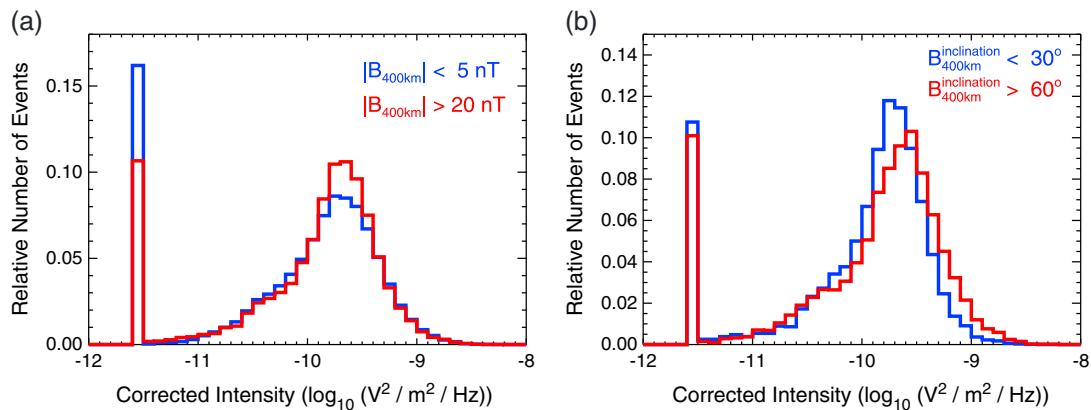
Figure 5. (a) Histograms of corrected intensities of ground traces measured at locations with model crustal magnetic field magnitude at 400 km lower than 5 nT/larger than 20 nT are shown in blue and in red, respectively. (b) Histograms of corrected intensities of ground traces measured at locations with model crustal magnetic field inclination at 400 km lower than 30°/larger than 60° are shown in blue and in red, respectively. Only ground traces measured at locations with model crustal magnetic field magnitudes larger than 20 nT were considered in this panel. Note that ground trace intensities equal to zero were set to the minimum nonzero histogram value to allow a representation using the log scale. This is the reason for high relative numbers of events in the bins on the left.

data point, and we normalize the corrected intensity by this median value. In very rare cases when there are less than 100 neighboring data points, the normalization is not done, and the corresponding data point is ignored in further analysis. The effect of this normalization procedure is shown in Figure 4. Figure 4a shows geographic locations where all the analyzed ionograms were measured. Color coded using the scale at the top is the corrected intensity of the ground traces observed at individual locations. Figure 4b uses the same representation, but for the normalized corrected ground trace intensities. It can be seen that the applied procedure leads to a more uniform geographic distribution of trace intensities, as expected.

Altogether, the resulting data set consists from 110,386 data points measured between June 2005 and June 2013 at SZA > 107°. Out of these, 16,297 data points have zero intensities. The normalized intensities of the remaining data points range from about 0.01 to 100.

3. Results

The normalization of ground trace intensities by the median intensity of neighboring data points effectively removes any variation on small spatial scales. This means that, among others, it removes also a possible dependence of ground trace intensities on the configuration of the crustal magnetic field. In order to verify a possible influence of the crustal magnetic field at a given place, one must therefore use nonnormalized corrected intensities. However, it should be noted that in such a case the varying overall surface reflectivity is possibly affecting the results. In other words, we cannot be sure whether a possible dependence would be due to crustal magnetic fields or due to geographic variations of the overall surface reflectivity. It is not possible to distinguish between these two possibilities.

A possible effect of crustal magnetic fields on the ground trace intensity is investigated in Figure 5. We have used the *Cain et al.* [2003] magnetic field model evaluated at an altitude of 400 km. Figure 5a shows a histogram of corrected intensities at locations with model magnetic field magnitude lower than 5 nT in blue, and a histogram of corrected intensities at locations with model magnetic field magnitude larger than 20 nT in red. The numbers of events in individual histogram bins were normalized by the total number of events, which allows us to easily compare the shape of histograms with different total numbers of events. We also note that ground trace intensities equal to zero were set to the minimum nonzero histogram value in order to allow a representation using the log scale. This is the reason for high relative number of events in the bin on the left. The same approach was used in all the following histograms. It allows us to efficiently deal with zero intensity ground traces, i.e., with the ground traces whose intensity principally corresponds to the noise-only situation because of too large attenuation of the reflected signal in the ionosphere. Although these data points do not contain any quantitative information (how large the attenuation was), they contain an important piece of qualitative information (it was large enough to prevent the reflected signal from being detected), and they thus should not be excluded from the analysis. It can be seen that both histograms basically overlap, indicating that the ground trace intensity is nearly independent on the magnetic field magnitude. However, it
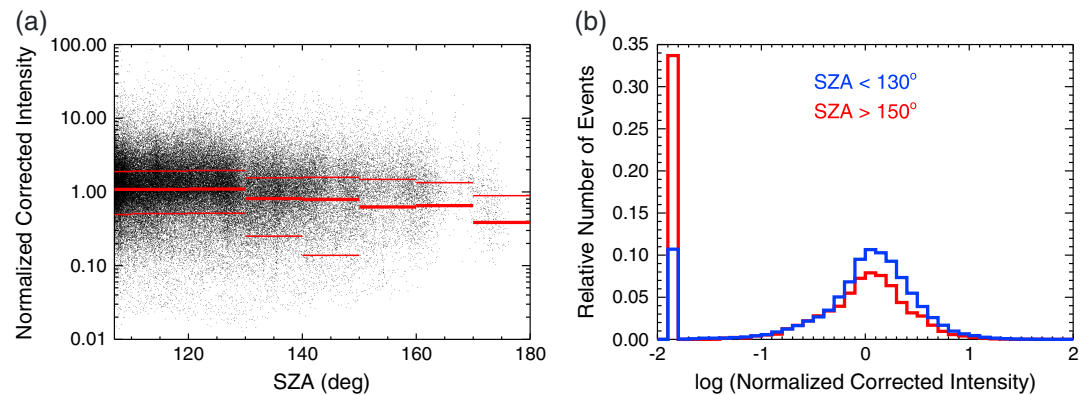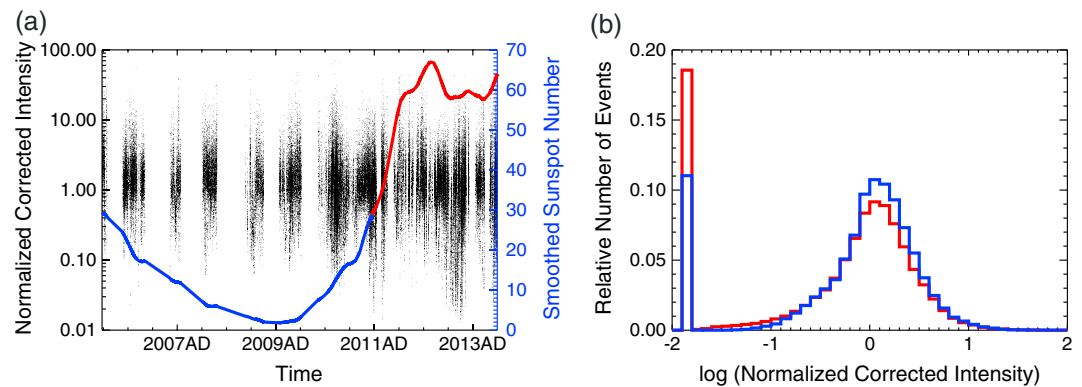
Figure 6. (a) Normalized corrected intensities of ground traces as a function of SZA. Median values calculated over given SZA intervals are shown by thick solid red lines, and 0.25 and 0.75 quartiles calculated over the same SZA intervals are shown by thinner solid red lines. Note that the three missing 0.25 quartile lines at large SZAs are due to the quartile intensities in these bins equal to zero, and therefore not shown on the used log scale. (b) Histograms of normalized corrected intensities of ground traces obtained at SZA < 130° and SZA > 150° are shown in blue and in red, respectively. Similarly as in Figure 5, ground trace intensities equal to zero were set to the minimum nonzero histogram value to allow a representation using the log scale.

is noteworthy that the percentage of zero-intensity ground traces (i.e., ionograms with no surface reflection signature) is higher by about 50% at locations with weak crustal magnetic field than at locations with strong crustal magnetic field.

Figure 5b uses the same format as Figure 5a, but this time the effect of the model crustal magnetic field inclination is analyzed. Because the magnetic field inclination becomes meaningless for weak crustal magnetic field, we have limited the analysis only to magnetic field magnitudes larger than 20 nT. The resulting histogram of corrected intensities of ground traces measured at locations with magnetic field inclination lower than 30° is shown in blue, and the resulting histogram of corrected intensities of ground traces measured at locations with magnetic field inclination larger than 60° is shown in red. It can be seen that there is a systematic difference between the two histograms, with the red histogram shifted toward larger intensities by about 0.8 dB. Although this shift is not very large compared to the width of the histograms, taking into account the enormous number of included data points it is clearly significant. Ground trace intensities at locations with highly inclined (i.e., nearly vertical) crustal magnetic field are therefore on average larger than ground trace intensities at locations with lowly inclined (i.e., nearly horizontal) crustal magnetic field.

The intensity of the ground traces as a function of SZA is analyzed in Figure 6. As small spatial scale variations are not of interest for this dependence, we use, similarly as for all remaining plots in the manuscript, the normalized corrected intensity of the ground traces. Figure 6a shows the normalized corrected intensities of ground traces as a function of SZA. Median values calculated over given SZA intervals are shown by thick solid red lines, and 0.25 and 0.75 quartiles calculated over the same SZA intervals are shown by thinner solid red lines. Note that the three missing 0.25 quartile lines at large SZAs are due to the quartile intensities in these bins equal to zero, and therefore not shown on the used log scale. It can be seen that there is a rather weak, but systematic trend for the normalized corrected intensity to decrease with increasing SZA. This is confirmed in Figure 6b, which shows histograms of normalized corrected intensities of ground traces obtained at SZA < 130° and at SZA > 150° in blue and in red, respectively. The median value of normalized corrected ground trace intensities at SZA > 150° is lower by about 2.7 dB than the median value of normalized corrected ground trace intensities at SZA < 130°. Moreover, the percentage of zero-intensity ground traces is more than three times higher at large SZAs as compared to lower SZAs.
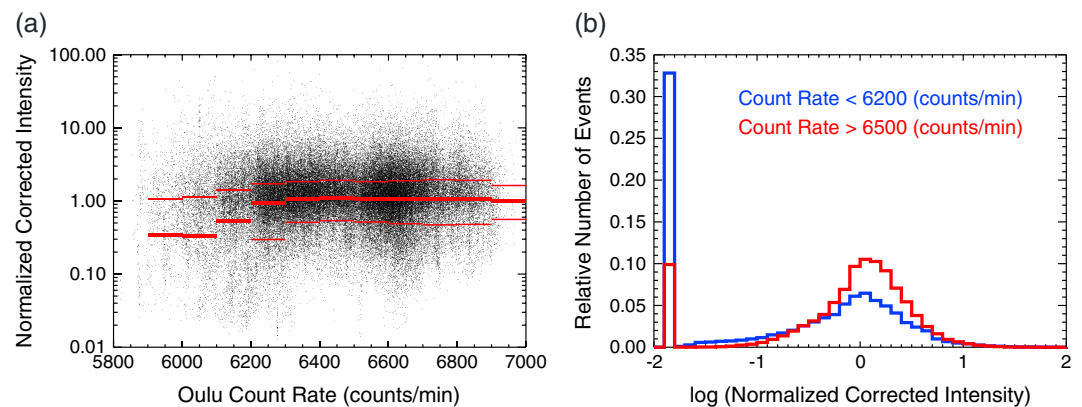
Having investigated the dependence of ground trace intensities on the spacecraft location, we focus on how the trace intensity is influenced by temporal variations, namely, by the solar activity. This is characterized by smoothed monthly mean sunspot number (http://www.sidc.be/silso/datafiles) in Figure 7. Figure 7a shows normalized corrected intensities as a function of time. Overplotted by the thick solid line is the smoothed monthly mean sunspot number. We have divided the data into two groups, distinguished by colors, corresponding approximately to solar minimum (blue part of the thick solid curve) and solar maximum (red part

Figure 7. (a) Normalized corrected intensities of ground traces as a function of time. Overplotted by the thick solid curve is the smoothed monthly mean sunspot number. The blue part of the line corresponds to the low solar activity, while the red part of the line corresponds to the high solar activity. (b) Histograms of normalized corrected intensities of ground traces obtained for low solar activity and for high solar activity intervals are shown in blue and in red, respectively. Similarly as in Figure 5, ground trace intensities equal to zero were set to the minimum nonzero histogram value to allow a representation using the log scale.

of the thick solid curve). Histograms of normalized corrected intensities of ground traces corresponding to the times of low and high solar activity are shown in Figure 7b in blue and in red, respectively. It can be seen that the two histograms are roughly comparable, but the red one is slightly shifted toward lower ground trace intensities. Namely, the median value of normalized corrected ground trace intensities obtained during the times of high solar activity is lower by about 0.9 dB than the median value of normalized corrected ground trace intensities obtained during the times of low solar activity.

The trend of lower ground trace intensities during larger solar activity is further confirmed in Figure 8. We use the neutron count rate from the neutron monitor in Oulu, Finland, to measure cosmic ray intensities at Earth (http://cosmicrays.oulu.fi). Galactic cosmic ray intensities vary with phase opposite to that of solar activity (see, e.g., the review by *Jokipii*, [2008]). During a solar maximum, fewer cosmic rays are detected at Earth, and, by extension, at Mars. Figure 8a shows normalized corrected intensities of ground traces as a function of the cosmic ray count rate. Median values calculated over given count rate intervals are shown by thick solid red lines, and 0.25 and 0.75 quartiles calculated over the same count rate intervals are shown by thinner solid red lines. It can be seen that the ground trace intensities measured at the times of low cosmic ray count rates are lower than usual. This is confirmed in Figure 8b, which shows histograms of normalized corrected intensities of ground traces obtained during the times when the count rate was lower than 6200 counts/min and larger than

Figure 8. (a) Normalized corrected intensities of ground traces as a function of the cosmic ray count rate. Median values calculated over given count rate intervals are shown by thick solid red lines, and 0.25 and 0.75 quartiles calculated over the same count rate intervals are shown by thinner solid red lines. (b) Histograms of normalized corrected intensities of ground traces obtained for cosmic ray count rates lower than 6200 counts/min and for cosmic ray count rates larger than 6500 counts/min are shown in blue and in red, respectively. Similarly as in Figure 5, ground trace intensities equal to zero were set to the minimum nonzero histogram value to allow a representation using the log scale.
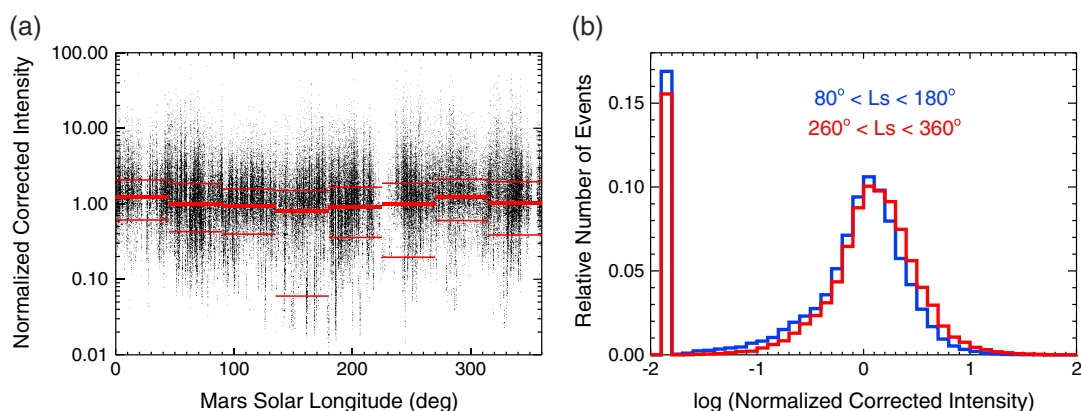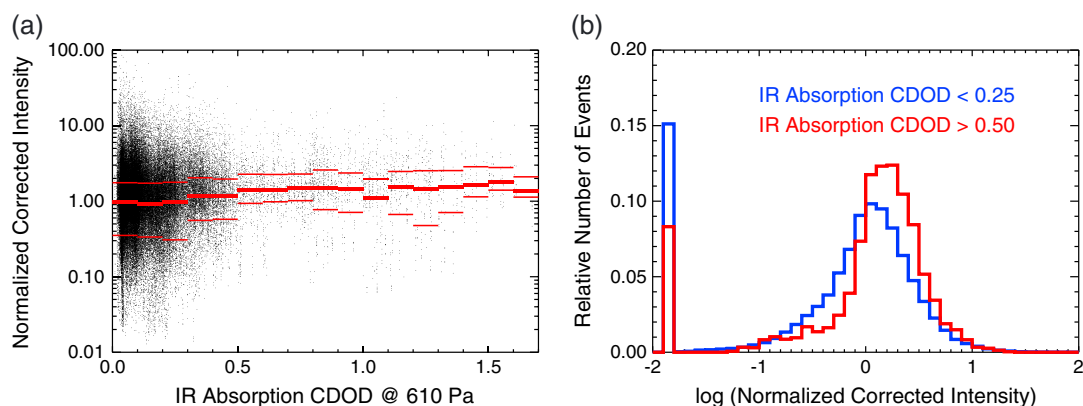
Figure 9. (a) Normalized corrected intensities of ground traces as a function of the Mars solar longitude (Ls). Median values calculated over given longitudinal intervals are shown by thick solid red lines, and 0.25 and 0.75 quartiles calculated over the same longitudinal intervals are shown by thinner solid red lines. (b) Histograms of normalized corrected intensities of ground traces obtained for 80° < Ls < 180° and for 260° < Ls < 360° are shown in blue and in red, respectively. Similarly as in Figure 5, ground trace intensities equal to zero were set to the minimum nonzero histogram value to allow a representation using the log scale.

6500 counts/min in blue and in red, respectively. The median values of normalized corrected ground trace intensities obtained during the times of low/large counts differ by about 4.2 dB. Moreover, the percentage of zero-intensity ground traces is more than 3 times higher during the times of low cosmic ray count rates than during the times of high cosmic ray count rates.

Three additional parameters possibly controlling the ground trace intensity were investigated. First, we have verified whether a magnetic shadow effect [e.g., *Kallio et al.*, 2012; *McKenna-Lawlor et al.*, 2012] can be identified in our data set. This should be the case if the electron densities at low altitudes were due to high-energy particles coming from the Sun approximately along the Parker spiral [*Luhmann et al.*, 2007]. We have used the same approach as successfully employed by *Němec et al.* [2014] for SEP time intervals, i.e., we analyzed the dependence on a distance from the mean Parker spiral shadow location in degrees. However, the ground trace intensities do not seem to depend on this parameter (not shown). Second, we have investigated the dependence of ground trace intensities on the Martian season expressed by the Mars solar longitude (Ls). The obtained results are shown in Figure 9. Figure 9a shows normalized corrected intensities of ground traces as a function of Ls. Median values calculated over given longitudinal intervals are shown by thick solid red lines, and 0.25 and 0.75 quartiles calculated over the same intervals are shown by thinner solid red lines. It can be seen that the ground trace intensities as a function of Ls exhibit a rather weak, but clearly pronounced periodic behavior. Specifically, the ground trace intensities appear to be larger at Ls around 300°. This is confirmed in Figure 9b, which shows histograms of normalized corrected ground trace intensities obtained at 80° < Ls < 180° and at 260° < Ls < 360° in blue and in red, respectively. The median values of normalized corrected ground trace intensities obtained at these two Ls ranges differ by about 0.9 dB. Third, we analyzed the dependence of ground trace intensities on the dust opacity expressed by the 9.3 μm absorption column dust optical depth (CDOD) normalized to 610 Pa [*Montabone et al.*, 2015]. We used daily maps compiled by *Montabone et al.* [2015] by combining various data sources (http://www-mars.lmd.jussieu.fr/mars/dust_climatology) to determine CDOD at the time and position of each analyzed MARSIS ground trace. Figure 10a then shows normalized corrected intensities of ground traces as a function of CDOD. Median values calculated over given intervals are shown by thick solid red lines, and 0.25 and 0.75 quartiles calculated over the same intervals are shown by thinner solid red lines. It can be seen that although the number of data points obtained at the times of large CDODs is rather small, these data points typically correspond to larger ground trace intensities. This is further confirmed in Figure 10b, which shows histograms of normalized corrected ground trace intensities obtained at the times of CDOD < 0.25 and at the times of CDOD > 0.5 in blue and in red, respectively. The median values of normalized corrected ground trace intensities obtained at these two CDOD ranges differ by about 1.7 dB.

The peak electron densities in the nightside ionosphere are usually too low to be detected by the MARSIS radar sounder, and the reflection from the nightside ionosphere is thus observable in only about 10% of nightside ionograms [*Němec et al.*, 2010]. At the times when MARSIS observes nightside ionospheric reflections, the peak electron density is therefore exceptionally large, likely due to the electron impact ionization along open
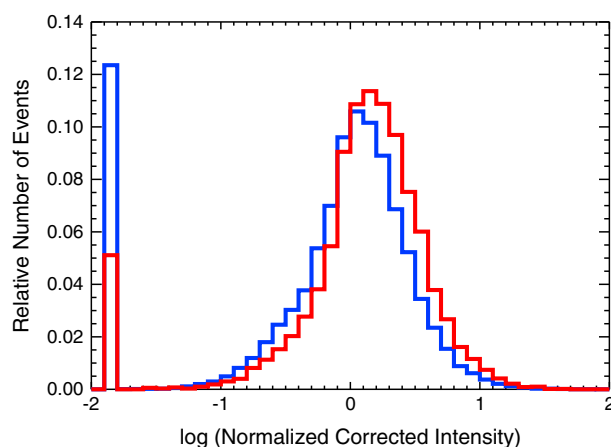
Figure 10. (a) Normalized corrected intensities of ground traces as a function of the 9.3μm absorption column dust optical depth (CDOD) normalized to 610 Pa [*Montabone et al.*, 2015]. Median values calculated over given intervals are shown by thick solid red lines, and 0.25 and 0.75 quartiles calculated over the same intervals are shown by thinner solid red lines. (b) Histograms of normalized corrected intensities of ground traces obtained at the times of CDOD < 0.25 and at the times of CDOD > 0.5 are shown in blue and in red, respectively. Similarly as in Figure 5, ground trace intensities equal to zero were set to the minimum nonzero histogram value to allow a representation using the log scale.

magnetic field lines [*Němec et al.*, 2011]. The relationship between the occurrence of nightside ionospheric reflections and the normalized corrected intensities of ground traces is analyzed in Figure 11. The histogram of normalized corrected intensities of ground traces obtained during the times when no nightside ionospheric reflections were detected is shown in blue. The histogram of normalized corrected intensities obtained during the times when nightside ionospheric reflections were detectable is shown in red. It can be seen that the red histogram is noticeably shifted toward larger ground trace intensity values, by about 1.4 dB when the median values are considered. It means that at the times when the ionospheric peak electron density is exceptionally large, the two-way ionospheric attenuation of the sounding signal is lower than expected. This is a surprising effect, indicating that the electron densities at low altitudes (responsible for the attenuation) are anticorrelated with the electron densities at higher altitudes (responsible for ionospheric reflections).

4. Discussion

The procedure developed for the evaluation of ground trace intensities, although rather simple, performs reasonably well. This has been tested by a comparison with randomly chosen MARSIS ionograms, and, moreover,

by the fact that ground trace intensities obtained for the SEP time intervals are essentially always equal to zero (not shown), in agreement with former results [*Němec et al.*, 2014]. However, the presented dependencies of ground trace intensities on several identified controlling factors suffer from a large scatter of the intensity values. This scatter is typically larger than the effect due to the change of the controlling variable, and it seems to be intrinsic for the performed analysis, with no way to improve it.

We believe that this scatter might be related to two principal factors affecting the ground trace intensity that we cannot properly account for: (i) The surface reflectivity changes significantly even on small spatial scales, both because of varying surface roughness and difficult geometry of reflecting radar signal [*Liu et al.*,

Figure 11. Histogram of normalized corrected intensities of ground traces obtained during the times when no nightside ionospheric reflections were detected is shown in blue. Histogram of normalized corrected intensities obtained during the times when nightside ionospheric reflections were detectable is shown in red. Similarly as in Figure 5, ground trace intensities equal to zero were set to the minimum nonzero histogram value to allow a representation using the log scale.

2014]; and (ii) the nightside ionosphere is very patchy [*Gurnett et al.*, 2008; *Němec et al.*, 2011]. This has been demonstrated for higher altitudes, but it is possibly the case also at lower altitudes where most of the signal attenuation takes place. Moreover, the low-altitude ionosphere may be affected by additional transient factors, such as dust storms [*Haider et al.*, 2010] and meteoroids [*Pätzold et al.*, 2005; *Withers et al.*, 2008], which are expected to further increase its spatial variability. These small-scale variations of ground trace intensities thus cannot be properly parametrized and accounted for in our analysis. Moreover, taking into account that a single MARSIS ionogram is not measured at once, but during a 1.26 s long time interval, small-scale variations are rather intrinsic for the analyzed data set. Finally, as we posses only a vertically integrated characteristic of the ionosphere, we are not able to distinguish how much the electron density was increased at a given altitude, and we have no information about the density profiles. We are thus not able to distinguish among many different factors possibly acting at the same time, necessarily resulting in the large scatter of the data points. However, taking into account the large number of analyzed data points, the large intensity scatter does not prevent us from obtaining statistically significant global dependencies on relevant controlling factors.

Before proceeding to a more detailed discussion of the obtained dependencies, we would like to underline the connection between ground trace intensities and electron densities at low altitudes. Nightside peak electron densities were shown to be lower than $10^4 cm^{-3}$ in the vast majority of events [*Němec et al.*, 2010]. Although the experimental determination of peak altitudes is rather problematic, recent theoretical studies agree on peak altitudes of about 160 km [*Fillingim et al.*, 2007; *Lillis et al.*, 2009]. Considering the attenuation calculations performed by *Withers* [2011], the attenuation of the sounding signal at the frequency of 5 MHz in the main ionospheric layer should be therefore about 0.001 dB, i.e., basically negligible. On the other hand, electron densities as low as a $100 cm^{-3}$ can result in 1 dB attenuation when located at altitudes of about 60 km. Consequently, we believe that the observed variations of ground trace intensities are mostly due to varying electron densities at these low altitudes. Nightside ground trace intensities can thus serve as a proxy for electron densities at low altitudes on the nightside, a region with principally no other experimental information available. Although a conversion of ground trace intensities to electron densities is not possible, as we possess only an integral characteristic of the region, it is reasonable to assume that lower intensities of ground traces correspond to larger electron densities at low altitudes. These, in turn, are believed to be due to impact ionization by precipitating energetic particles, most likely ions (as electrons are responsible for ionization at higher altitudes). Such a scheme was successfully demonstrated for SEP events [*Withers et al.*, 2012; *Němec et al.*, 2014], but it can be likely generalized and extended even to non-SEP intervals. The energy of the precipitating protons must be larger than about 1 MeV in order to cause an ionization at altitudes below 100 km [*Sheel et al.*, 2012].

The magnitude of the crustal magnetic field has only a weak effect on observed ground trace intensities. However, the slightly lower ground trace intensities observed at locations with weak crustal magnetic field (most importantly higher percentage of ground trace intensities equal to zero) indicate that the ionization source has a better access to low altitudes at these regions. This suggests that some (albeit rather small) portion of the ionization responsible for the attenuation of the sounding signal is due to lower energy energetic particles, as protons with energies larger than 83 MeV are almost unaffected by crustal magnetic fields [*Leblanc et al.*, 2002]. A possible candidate might be low-energy (less than 10 MeV) interplanetary ions, observed principally always, even during quiet times. The fact that their intensities are larger by an order of magnitude at solar maximum than at solar minimum [e.g., *Richardson et al.*, 1990] could then explain lower ground trace intensities (larger electron densities at low altitudes) obtained during larger solar activity. This result is not surprising, and it is consistent and presents a natural extension of formerly obtained results [*Morgan et al.*, 2006; *Espley et al.*, 2007; *Morgan et al.*, 2010; *Němec et al.*, 2014; *Morgan et al.*, 2014]. However, the absence of the magnetic shadow effect would suggest that the energetic ions responsible for the low-altitude ionization do not come from the Sun along the Parker spiral. The lack of the dependence of the ground trace intensities on the Parker spiral direction could be related to the observations of nearly isotropic distributions of low energy (< 10MeV) interplanetary ions [e.g., *Richardson et al.*, 1990]. It was suggested that such nearly isotropic ion distributions may result from particles originally streaming from the Sun along the Parker spiral, which were subsequently scattered by magnetic field irregularities in the interplanetary medium.

The dependence of ground trace intensities on the Martian season can be possibly related to the seasonal variation of the dust storm occurrence. Dust storm occurrence peaks in the so-called dust storm season around/just after the perihelion, which occurs at Ls ≈ 251°. The interval of Martian solar longitudes with larger ground trace intensities thus approximately corresponds to the period of increased dust storm occur-

rence. These seasonal variation results are thus in perfect agreement with the results obtained for the dust opacity, which show that larger CDODs typically correspond to larger ground trace intensities. This might be consistent with the results of *Haider et al.* [2010], who reported that during a dust storm a decrease of the ion concentrations resulting from ionization by galactic cosmic rays may appear in the lower region of the Martian ionosphere. This result is consistent with the study of aerosol charging in the Martian atmosphere by *Michael et al.* [2008], who showed that both ion and electron densities resulting from ionization by galactic cosmic rays are decreased close to the surface (below about 40 km altitude) when they become attached to aerosols during dust storms. This would, in turn, result in lower attenuation of the sounding signal, and therefore larger ground trace intensities. We note that ions with energies > 10MeV may reach altitudes below 50 km [e.g., *Sheel et al.*, 2012], so the results obtained by *Haider et al.* [2010] and *Michael et al.* [2008] may be applicable to ion and electron densities due to ionization by > 10MeV SEPs.

The obtained results show that ground trace intensities are on average lower at larger SZAs, indicating an increased ionization at low altitudes. Most importantly, the percentage of MARSIS ionograms with the signal attenuation too large for the surface reflection to be observed is about 3 times higher at SZA > 150° than at SZA < 130°. Assuming that the plasma responsible for the attenuation is produced locally, this indicates that the number of precipitating energetic ions is larger in high-SZA regions. It is not clear why this should be the case. Magnetic reconnection likely takes place in the Martian magnetotail [*Brain et al.*, 2006; *Eastwood et al.*, 2008; *Halekas et al.*, 2009; *Eastwood et al.*, 2012], being an additional energy source in this region. However, simulation results suggest that the ions energized during the reconnection would reach energies on the order of only about keV [*Harnett*, 2009], i.e., not sufficient to cause the ionization at low altitudes. Another possible explanation might possibly be the plasma circulation pattern around the planet. However, at the moment, we are not able to reliably explain the observed SZA dependence of ground trace intensities.

The ionization in the main nightside ionospheric layer is generally higher at locations with open (and typically more inclined) magnetic field lines [*Němec et al.*, 2010, 2011; *Cartacci et al.*, 2013] due to the impact ionization by energetic electrons precipitating in these regions [*Fillingim et al.*, 2007; *Lillis et al.*, 2009]. However, surprisingly and unexpectedly, ground trace intensities observed at these locations are generally larger than elsewhere, which indicates lower ionization at low altitudes. In order to get at least a qualitative explanation of this phenomenon, one needs to consider different mechanisms likely responsible for the ionization at different altitudes. The ionization in the main layer is due to energetic electrons precipitating in areas of open magnetic field lines. These electrons are, because of their comparatively small gyroradius, effectively guided by the magnetic field. On the other hand, energetic ions primarily responsible for the ionization at lower altitudes precipitate nearly unaffected by the magnetic field, i.e., there is much less reason for the low-altitude ionization to be larger at the areas with open magnetic field lines. However, this is still not sufficient to explain why the low-altitude ionization at these areas appears to be lower than elsewhere.

We believe that there might be two possible explanations. First, although the magnetic field does not much influence impinging high energy ions, it will influence significantly the resulting plasma at low altitudes. It seems plausible that in the areas of stronger and preferentially horizontal magnetic field, this plasma is more likely preserved, as it is effectively confined to a given location, preventing plasma outflow into space. This means that the precipitation of > MeV protons should not depend much on the crustal field orientation, while the outflow would not be compensated in regions of vertical magnetic field, causing lower plasma densities at low altitudes compared to regions of horizontal magnetic field. This would, however, require a significant plasma transport taking place. Second, the electrons impinging in areas with open magnetic field configuration can possibly heat the ionosphere. This heating was suggested as an explanation for the ionospheric bulges identified using oblique radar reflections [*Gurnett et al.*, 2005; *Duru et al.*, 2006; *Andrews et al.*, 2014]. The increased scale height would then lead to the expansion of the ionosphere to higher altitudes. This could, in turn, result in lower electron-neutral collision frequencies, and thus in lower signal attenuation in the ionosphere. It should be noted, however, that the dependence of the electron-neutral collision frequency is rather complicated. Namely, it includes a momentum transfer coefficient, which is equal to the product of the electron thermal speed and the electron-neutral collision cross section. These are both temperature dependent. However, the temperature dependence of the momentum transfer coefficient is rather small, and it can be in the first approximation neglected [*Withers*, 2011, and references therein].

5. Conclusions

We have presented an analysis of the intensity of nightside surface reflections measured by the MARSIS ionospheric radar sounder on board the Mars Express spacecraft. We have accounted for the varying spacecraft altitude and the varying surface reflectivity, and we analyzed the resulting normalized corrected intensity of ground traces as a function of several controlling parameters. The identified ground trace intensity variations are generally smaller than the intrinsic intensity scatter of individual data points. Nevertheless, taking into account the large number of analyzed data points, they are statistically significant and important for understanding the overall behavior. Taking into account that the electron densities in the nightside main ionospheric layer are too low to cause a significant attenuation of the sounding signal, the attenuation is expected to occur primarily at altitudes below about 100 km. The intensity of surface reflections can thus serve as a proxy for the electron density at low altitudes, which is a region not accessible by direct topside ionospheric sounding.

We have shown that the intensity of surface reflections is lower at higher solar zenith angles and during the periods of larger solar activity. We have also shown that the intensity of surface reflections exhibits a seasonal variation related to the dust storm occurrence. The intensity of surface reflections is higher in the areas of open magnetic field lines, which is further confirmed by comparison with simultaneous observations of the main ionospheric layer. Considering that larger ground trace intensities correspond to lower electron densities at low altitudes, this strongly suggests that nightside electron densities at low altitudes are anticorrelated with electron densities in the main ionospheric layer. We have suggested a possible explanation for this unexpected effect.

References

Andrews, D. J., M. André, H. J. Opgenoorth, N. J. T. Edberg, C. Diéval, F. Duru, D. A. Gurnett, D. Morgan, and O. Witasse (2014), Oblique reflections in the Mars Express MARSIS data set: Stable density structures in the Martian ionosphere, *J. Geophys. Res. Space Physics*, *119*, 3944–3960, doi:10.1002/2013JA019697.

Brain, D. A., J. S. Halekas, L. M. Peticolas, R. P. Lin, J. G. Luhmann, D. L. Mitchell, G. T. Delory, S. W. Bougher, M. H. Acuña, and H. Rème (2006), On the origin of aurorae on Mars, *J. Geophys. Res.*, *33*, L01201, doi:10.1029/2005GL024782.

Cain, J. C., B. B. Ferguson, and D. Mozzoni (2003), An n=90 internal potential function of the Martian crustal magnetic field, *J. Geophys. Res.*, *108*(E2), 5008, doi:10.1029/2000JE001487.

Cartacci, M., E. Amata, A. Cicchetti, R. Noschese, S. Giuppi, B. Langlais, A. Frigeri, R. Orosei, and G. Picardi (2013), Mars ionosphere total electron content analysis from MARSIS subsurface data, *Icarus*, *223*, 423–437.

Chicarro, A., P. Martin, and R. Trautner (2004), The Mars Express mission: An overview, in *Mars Express: The Scientific Payload, ESA Spec. Publ.*, vol. 1240, edited by A. Wilson and A. Chicarro, pp. 3–13, ESA Spec. Publ. Div., Noordwijk, Netherlands

Duru, F., D. A. Gurnett, T. F. Averkamp, D. L. Kirchner, R. L. Huff, A. M. Persoon, J. J. Plaut, and G. Picardi (2006), Magnetically controlled structures in the ionosphere of Mars, *J. Geophys. Res.*, *111*, A12204, doi:10.1029/2006JA011975.

Eastwood, J. P., D. A. Brain, J. S. Halekas, J. F. Drake, T. D. Phan, M. Øieroset, D. L. Mitchell, R. P. Lin, and M. Acuña (2008), Evidence for collisionless magnetic reconnection at Mars, *Geophys. Res. Lett.*, *35*, L02106, doi:10.1029/2007GL032289.

Eastwood, J. P., J. J. H. Videira, D. A. Brain, and J. S. Halekas (2012), A chain of magnetic flux ropes in the magnetotail of Mars, *Geophys. Res. Lett.*, *39*, L03104, doi:10.1029/2011GL050444.

Espley, J. R., W. H. Farrell, D. A. Brain, D. D. Morgan, B. Cantor, J. J. Plaut, M. H. Acuña, and G. Picardi (2007), Absorption of MARSIS radar signals: Solar energetic particles and the daytime ionosphere, *J. Geophys. Res.*, *34*, L09101, doi:10.1029/2006GL028829.

Fillingim, M. O., L. M. Peticolas, R. J. Lillis, D. A. Brain, J. S. Halekas, D. L. Mitchell, R. P. Lin, D. Lummerzheim, S. W. Bougher, and D. L. Kirchner (2007), Model calculations of electron precipitation induced ionization patches on the nightside of Mars, *Geophys. Res. Lett.*, *34*, L12101, doi:10.1029/2007GL029986.

Grima, C., W. Kofman, A. Herique, R. Orosei, and R. Seu (2012), Quantitative analysis of Mars surface radar reflectivity at 20 MHz, *Icarus*, *220*, 84–99.

Gurnett, D. A., et al. (2005), Radar soundings of the ionosphere of Mars, *Science*, *310*, 1929–1933.

Gurnett, D. A., et al. (2008), An overview of radar soundings of the Martian ionosphere from the Mars Express spacecraft, *Adv. Space Res.*, *41*, 1335–1346.

Haider, S. A., V. Sheel, M. D. Smith, W. C. Maguire, and G. J. Molina-Cuberos (2010), Effect of dust storms on the D Region of the Martian ionosphere: Atmospheric electricity, *J. Geophys. Res.*, *115*, A12336, doi:10.1029/2010JA016125.

Halekas, J. S., J. P. Eastwood, D. A. Brain, T. D. Phan, M. Øieroset, and R. P. Lin (2009), In situ observations of reconnection Hall magnetic fields at Mars: Evidence for ion diffusion region encounters, *J. Geophys. Res.*, *114*, A11204, doi:10.1029/2009JA014544.

Harnett, E. M. (2009), High-resolution multifluid simulations of flux ropes in the Martian magnetosphere, *J. Geophys. Res.*, *114*, A01208, doi:10.1029/2008JA013648.

Jokipii, J. R. (2008), Acceleration and transport of energetic particles observed in the inner heliosphere, *J. Atmos. Sol. Terr. Phys.*, *70*, 442–449.

Jordan, R., et al. (2009), The Mars Express MARSIS sounder instrument, *Planet. Space Sci.*, *57*, 1975–1986, doi:10.1016/j.pss.2009.09.016.

Kallio, E., S. McKenna-Lawlor, M. Alho, R. Jarvinen, S. Dyadechkin, and V. V. Afonin (2012), Energetic protons at Mars: Interpretation of SLED/Phobos-2 observations by a kinetic model, *Ann. Geophys.*, *30*, 1595–1609, doi:10.5194/angeo-30-1595-2012.

Leblanc, F., J. G. Luhmann, R. E. Johnson, and E. Chassefiere (2002), Some expected impacts of a solar energetic particle event at Mars, *J. Geophys. Res.*, *107*(A5), SIA 5-1–SIA 5-10, doi:10.1029/2001JA900178.

Lillis, R. J., M. O. Fillingim, L. M. Peticolas, D. A. Brain, R. P. Lin, and S. W. Bougher (2009), Nightside ionosphere of Mars: Modeling the effects of crustal magnetic fields and electron pitch angle distributions on electron impact ionization, *J. Geophys. Res.*, *114*, E11009, doi:10.1029/2009JE003379.

Liu, C., H. Ye, and Y.-Q. Jin (2014), Simulation of radar echoes from Mars' surface/subsurface and inversion of surface media parameters, *Radio Sci.*, *49*, 473–484, doi:10.1002/2013RS005367.

Luhmann, J. G., C. Zeitlin, R. Turner, D. A. Brain, D. Delory, J. G. Lyon, and W. Boynton (2007), Solar energetic particles in near-Mars space, *J. Geophys. Res.*, *112*, E10001, doi:10.1029/2006JE002886.

McKenna-Lawlor, S., E. Kallio, R. Jarvinen, and V. V. Afonin (2012), Magnetic shadowing of high energy ions at Mars and how this effect can be simulated using a hybrid model, *Earth Planets Space*, *64*, 247–256.

Michael, M., S. N. Tripathi, and S. K. Mishra (2008), Dust charging and electrical conductivity in the day and nighttime atmosphere of Mars, *J. Geophys. Res.*, *113*, E07010, doi:10.1029/2007JE003047.

Montabone, L., et al. (2015), Eight-year climatology of dust optical depth on Mars, *Icarus*, *251*, 65–95.

Morgan, D. D., D. A. Gurnett, D. L. Kirchner, R. L. Huff, D. A. Brain, W. V. Boynton, M. H. Acuña, J. J. Plaut, and G. Picardi (2006), Solar control of radar wave absorption by the Martian ionosphere, *Geophys. Res. Lett.*, *33*, L13202, doi:10.1029/2006GL026637.

Morgan, D. D., et al. (2010), Radar absorption due to a corotating interaction region encounter, *Icarus*, *206*, 95–103.

Morgan, D. D., O. Witasse, E. Nielsen, D. A. Gurnett, F. Duru, and D. L. Kirchner (2013), The processing of electron density profiles from the Mars Express MARSIS topside sounder, *Radio Sci.*, *48*, 197–207, doi:10.1002/rds.20023.

Morgan, D. D., et al. (2014), Effects of a strong ICME on the Martian ionosphere as detected by Mars Express and Mars Odyssey, *J. Geophys. Res. Space Physics*, *119*, 5891–5908, doi:10.1002/2013JA019522.

Mouginot, J., W. Kofman, A. Safaeinili, and A. Herique (2008), Correction of the ionospheric distortion on the MARSIS surface sounding echoes, *Planet. Space Sci.*, *56*, 917–926.

Mouginot, J., A. Pommerol, W. Kofman, P. Beck, B. Schmitt, A. Herique, C. Grima, A. Safaeinili, and J. J. Plaut (2010), The 3–5 MHz global reflectivity map of Mars by MARSIS/Mars Express: Implications for the current inventory of subsurface H_2O, *Icarus*, *210*, 612–625.

Nielsen, E., D. D. Morgan, D. L. Kirchner, J. Plaut, and G. Picardi (2007), Absorption and reflection of radio waves in the Martian ionosphere, *Planet. Space Sci.*, *55*, 864–870.

Němec, F., D. D. Morgan, D. A. Gurnett, and F. Duru (2010), Nightside ionosphere of Mars: Radar soundings by the Mars Express spacecraft, *J. Geophys. Res.*, *115*, E12009, doi:10.1029/2010JE003663.

Němec, F., D. D. Morgan, D. A. Gurnett, and D. A. Brain (2011), Areas of enhanced ionization in the deep nightside ionosphere of Mars, *J. Geophys. Res.*, *116*, E06006, doi:10.1029/2011JE003804.

Němec, F., D. D. Morgan, C. Diéval, D. A. Gurnett, and Y. Futaana (2014), Enhanced ionization of the Martian nightside ionosphere during solar energetic particle events, *Geophys. Res. Lett.*, *41*, 793–798, doi:10.1002/2013GL058895.

Pätzold, M., S. Tellmann, B. Häusler, D. Hinson, R. Schaa, and G. L. Tyler (2005), A sporadic third layer in the ionosphere of Mars, *Science*, *310*, 837–839, doi:10.1126/science.1117755.

Picardi, G., et al. (2004), MARSIS: Mars advanced radar for subsurface and ionosphere sounding, in *Mars Express: The Scientific Payload, ESA Spec. Publ.*, vol. 1240, edited by A. Wilson and A. Chicarro, pp. 51–69, ESA Spec. Publ. Div., Noordwijk, Netherlands

Richardson, I. G., D. V. Reames, K.-P. Wenzel, and J. Rodriguez-Pacheco (1990), Quiet-time properties of low-energy (<10 MeV per nucleon) interplanetary ions during solar maximum and solar minimum, *Astrophys. J.*, *363*, L9–L12.

Safaeinili, A., W. Kofman, J.-F. Nouvel, A. Herique, and R. L. Jordan (2003), Impact of Mars ionosphere on orbital radar sounder operation and data processing, *Planet. Space Sci.*, *51*, 505–515.

Safaeinili, A., W. Kofman, J. Mouginot, Y. Gim, A. Herique, A. B. Ivanov, J. J. Plaut, and G. Picardi (2007), Estimation of the total electron content of the Martian ionosphere using radar sounder surface echoes, *Geophys. Res. Lett.*, *34*, L23204, doi:10.1029/2007GL032154.

Sheel, V., S. A. Haider, P. Withers, K. Kozarev, I. Jun, S. Kang, G. Gronoff, and C. S. Wedlund (2012), Numerical simulation of the effects of a solar energetic particle event on the ionosphere of Mars, *J. Geophys. Res.*, *117*, A05312, doi:10.1029/2011JA017455.

Witasse, O., J. F. Nouvel, J. P. Lebreton, and W. Kofman (2001), HF radio wave attenuation due to a meteoric layer in the atmosphere of Mars, *Geophys. Res. Lett.*, *28*(15), 3039–3042.

Withers, P. (2011), Attenuation of radio signals by the ionosphere of Mars: Theoretical development and application to MARSIS observations, *Radio Sci.*, *46*, RS2004, doi:10.1029/2010RS004450.

Withers, P., M. Mendillo, D. P. Hinson, and K. Cahoy (2008), Physical characteristics and occurrence rates of meteoric plasma layers detected in the Martian ionosphere by the Mars Global Surveyor Radio Science Experiment, *J. Geophys. Res.*, *113*, A12314, doi:10.1029/2008JA013636.

Withers, P., M. O. Fillingim, R. J. Lillis, B. Häusler, D. P. Hinson, G. L. Tyler, M. Pätzold, K. Peter, S. Tellmann, and O. Witasse (2012), Observations of the nightside ionosphere of Mars by the Mars Express Radio Science Experiment (MaRS), *J. Geophys. Res.*, *117*, A12307, doi:10.1029/2012JA018185.